Interface Functionalization of Photoelectrodes with Graphene for High Performance Dye-Sensitized Solar Cells

*Tao Chen, Weihua Hu, Junling Song, Guan Hong Guai, and Chang Ming Li**

The microstructures of photo- and counter-electrodes play critical roles in the performance of dye-sensitized solar cells (DSSCs). In particular, various interfaces, such as fluorinated-tin oxide (FTO)/TiO_2, TiO_2/TiO_2, and TiO_2/electrolyte, in DSSCs significantly affect the final power conversion efficiency (PCE). However, research has generally focused more on the design of various nanostructured semiconducting materials with emphasis on optimizing chemical or/and physical properties, and less on these interface functionalizations for performance improvement. This work explores a new application of graphene to modify the interface of FTO/TiO_2 to suppress charge recombination. In combination with interfaces functionalization of TiO_2/TiO_2 for low charge-transport resistance and high charge-transfer rate, the final PCE of DSSC is remarkably improved from 5.80% to 8.13%, achieving the highest efficiency in comparison to reported graphene/TiO_2-based DSSCs. The method of using graphene to functionalize the surface of FTO substrate provides a better alternative method to the conventional pre-treatment through hydrolyzing $TiCl_4$ and an approach to reduce the adverse effect of microstructural defect of conducting glass substrate for electronic devices.

1. Introduction

Dye-sensitized solar cells (DSSC) are considered a promising alternative to silicon based solar cells owing to their low fabrication cost and reasonably high power conversion efficiency (PCE).[1–8] Various advanced materials, with focus on the design of nanostructured semiconducting materials, have been extensively studied for use as photo- and counter-electrodes to improve the performance of DSSCs.[2,9–12] In DSSC operation, various interfaces in the photoelectrode play critical roles in charge separation and transport. Specifically, electrons generated from excited dye molecules are separated at the TiO_2/dye interface, then transported through the 3D network of TiO_2 nanoparticles to the collecting electrode; the interface between transparent conducting glass (such as F:SnO_2, FTO) and TiO_2 under the condition of favorable energy levels enables the final charge collection. Nonetheless, interfaces also pose adverse effects for high-performance DSSCs, since they are the primary location for charge/hole recombination; in addition to the interfaces mentioned above, charge recombination can also occur at FTO/electrolyte, FTO/TiO_2, and grain boundaries of FTO.[13,14] Notably, the predominant place for recombination in DSSCs is the FTO/TiO_2 surface.[14] Therefore, manipulating the competition between charge transport to collecting electrode and charge recombination on the locus is obviously a key requirement towards high performance DSSCs.

This work aims at reducing the recombination at the FTO/TiO_2 interface, as well as the grain boundaries of FTO, through surface modification of FTO by graphene. To date there has been no report on engineering the TiO_2/FTO interface to retard the interfacial recombination, nor on the mechanism involved. Relevant investigations were carried out by coating FTO surface with a thin layer of TiO_2 film via hydrolyzing $TiCl_4$ aqueous solution.[8] However, it is known that $TiCl_4$ is quite easy to hydrolyze when exposed to air and moisture, which makes the coating process difficult to handle. Therefore, there is a great need to develop new and facile alternative approaches for the $TiCl_4$-enabled TiO_2 coating process. As a 2D allotrope of carbon, graphene shows great potential in optoelectronic devices due to its remarkable electronic properties – electron transport in 2D graphene is just as massless relative particles.[15–17] Herein, for the first time we demonstrate that a graphene coating on FTO surface can significantly reduce charge recombination at FTO/TiO_2 surfaces. The rationality of this design is that, when a graphene sheet exists in between FTO and TiO_2, electrons can transport from TiO_2 to graphene but not in reverse, as the work function of graphene (–4.4 eV vs. vacuum) is more negative than the conduction band of TiO_2 (–4.2 eV vs. vacuum).[18–20] Further, due to the fact that the work function of graphene is

Dr. T. Chen,[+] W. Hu, J. Song, G. H. Guai, Prof. C. M. Li
School of Chemical and Biomedical Engineering and Center for Advanced Bionanosystems
Nanyang Technological University
70 Nanyang Drive, 637457, Singapore
E-mail: ecmli@ntu.edu.sg

W. Hu, Prof. C. Ming Li
Institute for Clean Energy & Advanced Materials
Southwest University
Chongqing 400715, P. R. China
E-mail: ecmli@swu.edu.cn

W. Hu, Prof. C. Ming Li
Chongqing Key Laboratory for Advanced Materials and Technologies of Clean Electrical Power Sources
Chongqing 400715, P. R. China

[+] Present address: Department of Physics, The Chinese University of Hong Kong, Shatin, Hong Kong, P. R. China

DOI: 10.1002/adfm.201201126

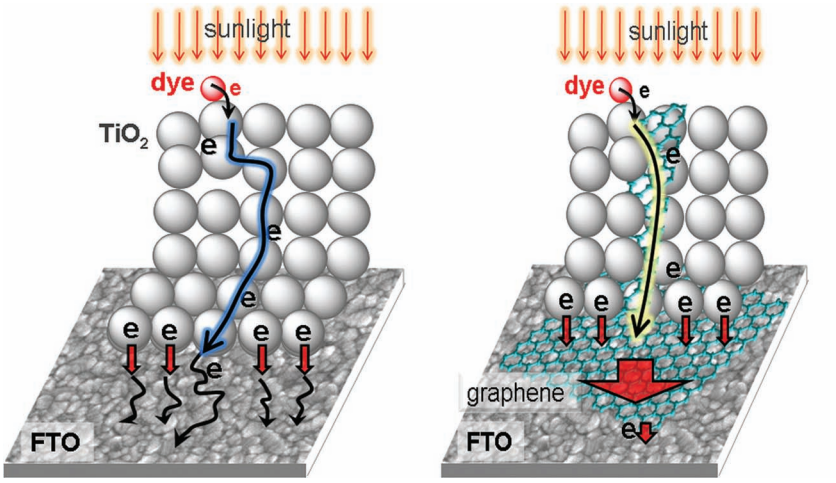

Scheme 1. Schematic illustration of the devices and electron transport path: a) depicting the reference DSSC with only TiO_2 nanoparticles as anode semiconducting materials and **N719** dye as sensitizer (the scheme is adapted from an SEM image of a real FTO, see Figure S4 in the Supporting Information and, b) illustrating DSSC with graphene as a interlayer of FTO/TiO_2 and in TiO_2 nanoparticle network. There is only one dye molecule in each scheme, for purposeof illustration only.

quite similar to that of FTO, the surface functionalization of FTO by graphene can behave as an extended collecting electrode (**Scheme 1**) to enhance the electron collection efficiency while significantly improving the charge-transport rate in the current collector.

2. Results and Discussion

Graphene-functionalized FTO was prepared by spin-coating, in which 50 µL of graphene (0.125 mg mL^{-1} in ethanol) was dispersed on the surface of FTO substrate with a spinning speed of 800 rpm for 1 min. To investigate the influence of the distribution density of the coated graphene on device performance, FTO surfaces were spin-coated 1, 2, or 3 times using the same spinning parameters, denoted as SC1, SC2, and SC3, respectively. The SEM image shows that graphene is well-dispersed on the surface FTO (**Figure 1**a). Further spin-coating of graphene on the FTO surface (SC2 and SC3) leads to higher surface coverage of graphene, with a size of 0.5–3 µm (Figure 1b,c). The fine structure of graphene on FTO surface in the high-magnification SEM image (Figure 1d) clearly displays a flat graphene coating on the FTO surface with a few wrinkle-like morphologies. It is also noted that the average diameter of FTO nanoparticles is 80 nm; thus, one graphene sheet can cover a number of FTO nanoparticles.

Transmittance was performed to study the optical properties of graphene-functionalized FTO substrate. The original FTO substrate shows a transmittance maximum of 84.6% at 651 nm (Figure 1e). After spin-coating of graphene for one cycle, the optical transmittance at 651 nm is slightly reduced to 83.7%. It is further reduced to 83.0% and 82.1% with two and three times spin-coating (Figure 1e). This observation indicates excellent optical transmittance of the coated graphene sheet, assuring good illumination of the dye molecules adsorbed on TiO_2 surface.

As well as being used for functionalization of the FTO surface, graphene was also used to form graphene/TiO_2 composite anodes to functionalize TiO_2. Different from mostly adopted methods, which typically involve mixing graphene with TiO_2 powders (P25) or connecting graphene and TiO_2 through functional molecules,[18–20] we prepared graphene/TiO_2 paste to improve the film formability for high-performance DSSCs. It was observed that the graphene/TiO_2 film thickness can reach 11 µm without cracking or peeling-off after annealing at

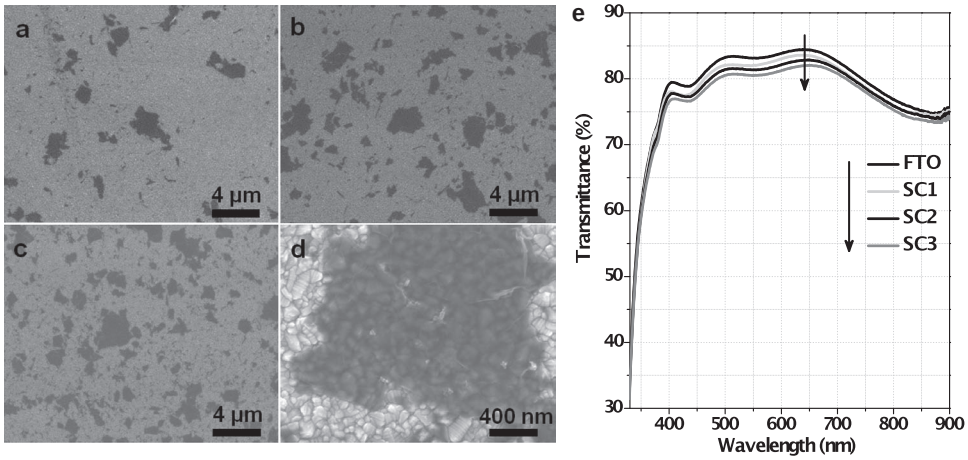

Figure 1. SEM images of FTO surfaces pretreated by graphene of device **3** (SC1, a), **4** (SC2, b), and **5** (SC3, c and d). e) UV-vis transmittance spectra of FTO without graphene functionalization and ofdevices **3** (SC1), **4** (SC2), and **5** (SC3).

Table 1. Performance parameters of the DSSCs operated under 1 Sun illumination.

Device[a)]	GS in TiO_2	GS on FTO[b)]	J_{sc} [mA cm^{-2}]	V_{oc} [V]	FF	PCE [%]
1	0%	0	15.20	0.714	0.53	5.80
2	0.02%	0	16.46	0.749	0.58	7.20
3	0.02%	SC1	19.43	0.744	0.54	7.74
4	0.02%	SC2	19.47	0.751	0.56	8.13
5	0.02%	SC3	18.54	0.744	0.54	7.40
6	0.02%	$TiCl_4$ pretreatment	19.26	0.742	0.53	7.54

[a)]Device **1** is a reference DSSC without graphene sheet incorporation; [b)]In Device **3**, **4**, and **5**, the FTO (anode) was pre-treated by spin-coating of graphene at a speed of 800 rpm with different cycles. The results are based on the average of 5 electrodes for each anode material. The effective area of each DSSC was 0.25 cm^2.

400 °C. For comparison, a baseline device (device **1**) was fabricated with only TiO_2 as the semiconducting anode materials on FTO surface without pre-modification by graphene. This device shows PCE of 5.80% (**Table 1**). We further optimized the graphene concentrations in graphene/TiO_2 paste, showing that the graphene concentration of 0.02 wt% achieves the best device performance (device **2**) with short-circuit current (J_{sc}), open-circuit voltage (V_{oc}) and PCE of 16.46 mA cm^{-2}, 0.749 V and 7.20%, respectively (optimization details are provided in the Supporting Information).

The optimized graphene/TiO_2 paste for device **2** was further used to fabricate devices with graphene-functionalized FTO substrates. DSSC (device **3**) fabricated with one-time spin-coated graphene on FTO delivered J_{sc}, V_{oc}, and *PCE* of 19.43 mA cm^{-2}, 0.744 V, and 7.74% (Table 1), respectively, of which *PCE* was higher than that of device **2** (η = 7.20%) without a graphene-functionalized FTO. After increasing the surface coverage of graphene by spin-coating twice (device **4**), the J_{sc}, V_{oc}, and *FF* of the DSSC increased to 19.47 mA cm^{-2}, 0.751 V, and 0.56, resulting in a PCE of 8.13%. These results clearly indicate that graphene-coated FTO surface can greatly elevate the energy conversion efficiency. However, with more graphene on the FTO surface (device **5**, three-times spin-coating), the PCE decreased to 7.40% (Table 1). The light utility of dyes decreased by a thick graphene coating on FTO is a possible reason for the PCE decrement;[21] a more detailed mechanism related to the energy conversion process will be discussed later.

It is established that a change of few ohms of interfacial resistance in photoelectrode could result in a great impact on DSSC performance, since a few percent of PCE improvement can be considered to be significant. To understand the performance enhancement mechanism of the graphene functionalization, electrochemical impedance spectra (EIS) of DSSCs are a powerful tool. It is known that the electrocatalytic behavior can be well characterized at the equivalent or open potential at which the exchange current between anodic and cathodic reaction and interfacial resistances can be measured without polarization interference.[22] In this work, EIS were measured at open-circuit potential (OCV) under 1 Sun illumination, as shown in the Nyquist plots (**Figure 2**), which display two well-defined semicircles. Quantitative analysis of EIS was conducted based on equivalent circuit (inset of Figure 2),[18,23–25] where R_s, R_1, and R_2 represent series resistance and charge-transfer resistances at counter electrode/electrolyte interface and at the TiO_2/dye/electrolyte interface, respectively.[26] The small and large semicircles in Figure 2 are attributed to charge transfer at the Pt/electrolyte and TiO_2/electrolyte interfaces (R_1 and R_2), respectively, while the intercept of the first circle on Z_{real}(R_s) is the Ohmic serial resistance (R_s) caused by electrolyte, electrodes, and other components such as FTO substrate, graphene coating, etc. The fitted parameters are summarized in **Table 2**. The charge transfer resistance of the mediate semicircles (R_2) of devices **3**, **4**, and **5** are 20.1, 18.9, and 19.8 Ω, respectively, which corresponds to the evolution of current density (Table 1). The R_2 of device **1** of TiO_2/electrolyte interface is 23.0 Ω, while that of device **2** is only 17.7 Ω. Since R_2 represents the charge transfer at the interface of TiO_2/dye/electrolyte, these results indicate that graphene incorporated into the TiO_2 network can enhance the charge-transfer rate.[13] This observation is further confirmed in devices **3**, **4**, and **5**, in which all the R_2s are smaller than that of device **1**.

Series resistance (R_s) is the resistance at $\omega = \infty$, which could represent the charge-transport and solution resistances in the electrode since identical counter-electrode and electrolyte are used in the experiments. As shown in Figure 2 and Table 2, with graphene incorporated in the TiO_2 nanoparticle network in device **2**, the R_s increased to 25.9 Ω. It is very hard to believe the charge-transport becomes sluggish after graphene incorporation. Thus, it is very likely that the graphene/TiO_2 paste-formed photoelectrode has high porosity when compared with the plain TiO_2, resulting in relatively slower mass transport in the electrode for higher solution resistance.[18] Nevertheless, R_s also increases with more graphene coated on the FTO surface from device **2** to **3**, **4**, and **5**, which may be caused by the

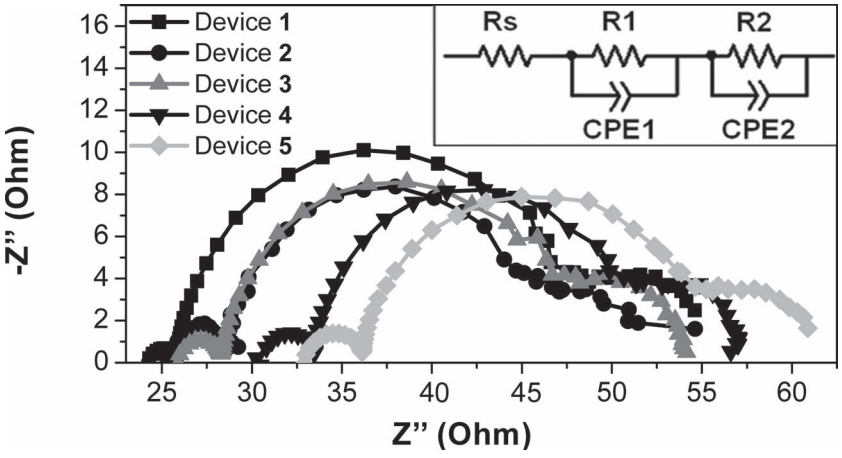

Figure 2. Electrochemical impedance spectra of device **1**, **2**, **3**, **4**, and **5** (the inset shows the equivalent circuit).

Table 2. Electrochemical impedance parameters of the DSSCs operated under 1 Sun illumination.

Device	R_s [a] [Ω]	R_2 [b] [Ω]	ω_{max} [c] [Hz]
1	24.2	23.0	48
2	25.3	17.7	45
3	25.9	20.1	44
4	30.4	18.9	43
5	32.9	19.8	47

[a]Sheet resistance; [b]charge- transfer resistance at TiO_2/dye–electrolyte interface; [c]calculated frequencies based on the mediate semicircles.

inefficient electronic/physical interaction between graphene and FTO,[14,27] leading to poor electron transport in the direction perpendicular to FTO/graphene interface. The increased series resistance for charge transport can be expected to partially offset the graphene-improved charge transfer at the electrode/electrolyte interfaces. On the other hand, the maximum frequency (ω_{max}) from the semicircle for device **1** is 48 Hz. With graphene modification, ω_{max} reduces to 45 Hz in device **2**. Since ω_{max} is inversely associated with electron lifetime (τ_e): $\tau_e = 1/(2\pi\omega_{max})$,[28,29] the decreased ω_{max} indicates a reduced rate of the charge-recombination process with graphene incorporated in the TiO_2 nanoparticle netwrok. The results above show that device **3** and **4** with graphene-functionalized FTO can further reduce the charge recombination rate. However, the high surface density of the graphene coating on FTO causes a shorter electron lifetime (device **5**); the high charge-transport resistance as discussed above for higher charge recombination should account for this variation. Therefore, appropriate surface coverage of graphene on the surface of FTO substrate is important for the efficient performance improvement of DSSCs.

Fundamentally, the performance of a DSSC is closely related to charge transfer at the electrode/electrolyte interface, charge recombination during the charge transport process and the charge transport rate in the bulk electrode/electrolyte for eventual charge separation and final charge collection, in which the most sluggish process is the rate-determining step that decides overall device performance. From the EIS results, the performance-enhancement mechanism can be analyzed. It is clear that the charge-transfer rate is the rate-determining step of the plain TiO_2 for the device performance, since all the graphene-functionalized TiO_2 electrodes increase the interface charge-transfer rate and improve the device performance. It is very likely that the charge recombination in the TiO_2/graphene electrode without the graphene-functionalized FTO becomes the rate-determining step, since devices **3** and **4** with the graphene-functionalized FTO show lower interfacial charge-transfer rate but higher charge recombination and eventually improve the power conversion efficiency greatly. The EIS also indicate that there is an optimal graphene coating on FTO. Too much graphene coating on FTO causes a low charge-transfer rate and high charge-transport resistance to become the rate-determining step again. Apparently, the graphene-functionalized FTO mainly retard the charge-recombination process to improve the DSSC device performance. Physical insight into the graphene coating on FTO retarding the charge recombination process is not apparent at present; this is currently under investigation in our laboratory.

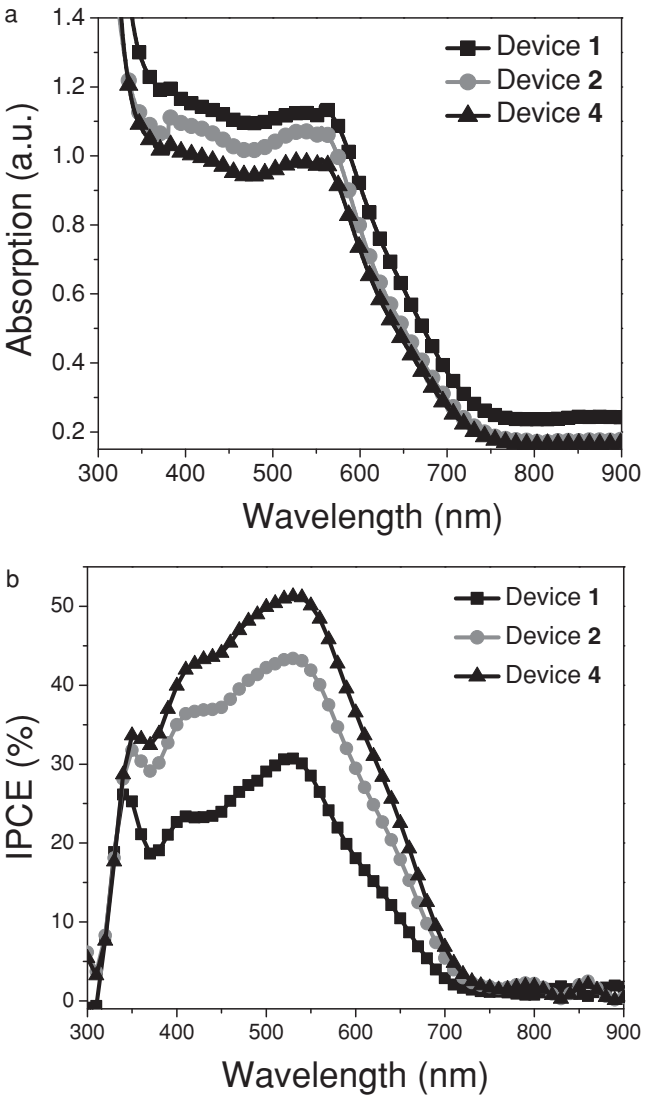

Figure 3. UV-vis absorption spectra (a) of dye-absorbed photoanodes and IPCEs (b) of devices **1**, **2**, and **4**.

Further investigation was carried out to study the absorption properties of the graphene/TiO_2 anode films. **Figure 3**a depicts the UV-vis absorption spectra of the graphene/TiO_2 anode films after dye absorption for 16 h of device **1**, **2**, and **4**. With graphene incorporation, the absorption in the range of 370–670 nm gradually decreases in device **1**, **2**, and **4**. However, incident photon-to-electron conversion efficiencies (IPCE) of the graphene-functionalized electrodes (Figure 3b) changed in contradiction to the absorption characteristics. At 530 nm, the IPCEs of devices **2** and **4** increase by factors of 1.41 and 1.67, respectively, over that of device **1**. IPCE is usually determined by dye loading capacity and charge collection at the collecting electrode. Since graphene incorporation causes a lower adsorption

efficiency, this result clearly indicates that it mainly enhances the charge collection at the collecting electrode. Graphene coating on TiO_2 could quickly capture and shuttle electrons to the collecting electrodes, which leads to the IPCE increment of device **2**.[30] Since devices **2** and **4** were made with the same graphene/TiO_2 paste, the ICPE improvement of device **4** should be mainly ascribed to the suppression of charge recombination on FTO surface with the graphene coating for more charge (electrons) collection. This result strongly supports the mechanism analysis based on the EIS data.

Parallel examination was performed using $TiCl_4$-pretreated FTO substrate to fabricate the photoanode (device **6**), which is often used as an effective approach to reduce the charge recombination on the conducting FTO surface by forming a thin layer of TiO_2.[8] After treatment in terms of the reported method,[8] the same graphene/TiO_2 paste as that in device **3**, **4**, and **5** was assembled on the $TiCl_4$-pretreated FTO surface followed by annealing to produce a graphene/TiO_2 anode film. A J_{sc} of 19.26 mA cm^{-2} and a V_{oc} of 0.742 V were achieved to produce an overall efficiency of 7.54%, which is smaller than that of device **4** (8.13%) utilizing graphene to functionalize the FTO surface. Therefore, using graphene-pretreated FTO as a photoanode offers a new, convenient, and more efficient approach to reduce the charge recombination on the FTO interface for higher device performance.

3. Conclusions

We have demonstrated a novel and efficient method to enhance the power conversion efficiency through reducing the charge recombination process occurred at the interface of FTO nanopaticles and FTO/TiO_2 by using graphene functionalization. The results show that the graphene functionalization of FTO surface is a better approach than the known surface modification by hydrolyzing $TiCl_4$ solution to improve the overall DSSC power conversion efficiency. Importantly, spin-coating graphene on FTO surface is simpler and more convenient than conventional $TiCl_4$ hydrolyzing. By using graphene to functionalize both interfaces of TiO_2/TiO_2 and TiO_2/FTO, a final power conversion efficiency was remarkably increased from 5.80% to 8.13%. The enhancement is mainly contributed from the improved charge transfer and retarded charge recombination by graphene-functionalized interfaces in the photoelectrode.

4. Experimental Section

Materials: Dye sensitizer *cis*-bis(isothicyanato)bis(2,2′-bipyridyl-4,4′-discarboxylato)-ruthenium(II)-bis-tetrabutylammonium, (coded as N719), TiO_2 paste (DSL 18NR-T) and iodide-based liquid electrolyte (HL-HPE) were purchased from Dyesol company.

Synthesis of Graphene and Graphene–TiO_2 Mixed Paste: Graphene was synthesized by reduction of graphene oxide, which was prepared by the modified Hummers method.[31,32] A mixture of graphite (2 g, Sigma Aldrich), concentrated HNO_3 (20 mL) and concentrated H_2SO_4 (60 mL) was vigorously stirred at 80 °C for 10 h. For oxidation, the mixture was treated with H_2O_2 (20 mL, 30 wt%) for 2 d, followed by filtering and washing with de-ionized (DI) water using a 0.22 micron Nylon Millipore filter to remove the residual acid. The product was then dried under ambient condition overnight. Afterward, a brief annealing of the obtained graphene oxide (GO) powder was carried out at 1000 °C for 1 min and cooled down to room temperature under argon. Thermally expanded GO was thus exfoliated by sonicating in water for 1 h. For preparation of graphene sheets, GO suspension was reduced by hydrazine (100 mL) for 24 h. The solution was centrifuged at 10 000 rpm for 10 min to form a homogenous graphene sheet solution and dried via evaporation of water at 60 °C. Finally, a portion of 10 mg of the as-prepared graphene sheets was washed copiously with ethanol and dispersed again in 20 mL of anhydrous ethanol by sonication for 4 h to form a well-dispersed graphene solution, which was used for preparing graphene/TiO_2 hybrid paste. The graphene/TiO_2 pastes were prepared by adding different volumes of graphene into TiO_2 paste (Ti-nanoxide HT/SP, Solaronix) to make a final weight percentage of 0.0089, 0.014, 0.020, and 0.029 wt% for devices **2**, **3**, **4**, and **5**, respectively. The mixture was sonicated at 70 °C for 2 h to render a uniform distribution of graphene in TiO_2 paste.

Device Fabrication: A doctor-blade technique was utilized to produce photoanode (TiO_2 or graphene/TiO_2) films. Briefly, transparent conducting glass (SnO_2:F, FTO, Nippon Glass Sheet, Japan, 12 Ω^{-1}) was cleaned in 5 wt% detergent using an ultrasonic bath for 30 min, followed by rinsing with DI water. The FTO glass was then immersed in DI water and sonicated for 10 min, followed by removing water. This procedure was repeated three times to thoroughly clean the surface of FTO. Then 11 μm thick TiO_2 or graphene/TiO_2 electrodes were doctor-bladed onto FTO or graphene functionalized FTO surfaces. It was relaxed at room temperature for 3 min before heating at 125 °C for 6 min. After that, the film was sintered at 350 °C for 20 min and 450 °C for 40 min, followed by cooling to room temperature. For the dye adsorption, the electrodes were immersed in 0.3 mM N719 dye in acetonitrile/tert-butyl alcohol (1:1 v/v) at room temperature for 16 h, followed by briefly rinsing with ethanol and drying in air.

Platinum counter electrodes were prepared by sputtering at 20 mA for 60 s at a power of 150 W. Two holes (0.75 mm diameters) were pre-drilled in the FTO glass for introducing electrolyte. After that, dye-adsorbed TiO_2 electrode and counter electrode were stacked and sealed with 60 μm thermal-plastic Suryln spacers at 115 °C for 12 s. The effective areas of the photoanodes were 0.25 cm^2. Iodide-based liquid electrolyte (HL-HPE, 0.1 M LiI, 50 mM I_2 and 0.6 M DMPII) was introduced into the sandwich cells through the drilled holes in the Pt electrode. Then it was sealed by parafilm at elevated temperature.

Characterization Methods: The morphology, cross-section of the graphene/TiO_2 film and energy-dispersive X-ray spectroscopy (EDS) analysis were conducted on a field-emission scanning electron microscopy (FESEM, Jeol JSM-6701F). TEM images of the as-synthesized graphene were collected from a JEM-1400 transmission electron microscope operated at 120 kV. UV-Vis absorption and transmittance of the anode films with and without dye adsorption were carried out using a UV-3600 Shimadzu UV-Vis spectrometer. A Newport solar simulator with AM 1.5G filter for illumination (100 mW cm^{-2}), the current–voltage (*J–V*) characteristics of the assembled cells were measured by a Keithley 2420 multimeter. Electrochemical impedance spectroscopy (EIS) was recorded under 1 Sun illumination over a frequency range of 0.01–105 Hz with an AC amplitude of 10 mV by using Solartron Analytical 1260 Impedance/Gain-phase analyzer connected with the 1294 Impedance Interface measuring unit. The parameters were calculated from Z-View software (v2.1b, Scribner Associate, Inc.). IPCEs of devices **1**, **4**, and **7** were recorded in Solar Cell QE/IPCE Measurement System (Zolix Solar Cell Scan 100) in DC mode.

Supporting Information

Supporting Information is available from the Wiley Online Library or from the author.

Acknowledgements

This work was supported by the Institute for Clean Energy & Advanced Materials, Southwest University, Chongqing 400715, P. R. China, and the

Agency for Science, Technology and Research (A*Star), Singapore under SERC Grant No. 072 134 0054.

Received: April 23, 2012
Published online: August 3, 2012

[1] M. Grätzel, *Acc. Chem. Res.* **2009**, *42*, 1788.
[2] A. Hagfeldt, G. Boschloo, L. Sun, L. Kloo, H. Pettersson, *Chem. Rev.* **2010**, *110*, 6595.
[3] L. M. Goncalves, V. D. Bermudez, H. A. Ribeiro, A. M. Mendes, *Energy Environ. Sci.* **2008**, *1*, 655.
[4] B. Oregan, M. Grätzel, *Nature* **1991**, *353*, 737.
[5] S. Muduli, W. Lee, V. Dhas, S. Mujawar, M. Dubey, K. Vijayamohanan, S. H. Han, S. Ogale, *ACS Appl. Mater. Interfaces* **2009**, *1*, 2030.
[6] S. Agarwala, M. Kevin, A. S. W. Wong, C. K. N. Peh, V. Thavasi, G. W. Ho, *ACS Appl. Mater. Interfaces* **2010**, *2*, 1844.
[7] J. Liu, Y.-T. Kuo, K. J. Klabunde, C. Rochford, J. Wu, J. Li, *ACS Appl. Mater. Interfaces* **2009**, *1*, 1645.
[8] S. Ito, T. N. Murakami, P. Comte, P. Liska, C. Gratzel, M. K. Nazeeruddin, M. Gratzel, *Thin Solid Films* **2008**, *516*, 4613.
[9] E. S. Kwak, W. Lee, N. G. Park, J. Kim, H. Lee, *Adv. Funct. Mater.* **2009**, *19*, 1093.
[10] J. D. Roy-Mayhew, D. J. Bozym, C. Punckt, I. A. Aksay, *ACS Nano* **2010**, *4*, 6203.
[11] T. Chen, G. H. Guai, C. Gong, W. H. Hu, J. X. Zhu, H. B. Yang, Q. Y. Yan, C. M. Li, *Energy Environ. Sci.* **2012**, *5*, 6294.
[12] F. Z. Huang, D. H. Chen, X. L. Zhang, R. A. Caruso, Y. B. Cheng, *Adv. Funct. Mater.* **2010**, *20*, 1301.
[13] A. J. Frank, N. Kopidakis, J. van de Lagemaat, *Coord. Chem. Rev.* **2004**, *248*, 1165.
[14] X. Wang, L. J. Zhi, K. Müllen, *Nano Lett.* **2008**, *8*, 323.
[15] C. X. Guo, G. H. Guai, C. M. Li, *Adv. Energy Mater.* **2011**, *1*, 448.
[16] C. N. R. Rao, A. K. Sood, K. S. Subrahmanyam, A. Govindaraj, *Angew. Chem. Int. Ed.* **2009**, *48*, 7752.
[17] M. Terrones, A. R. Botello-Mendez, J. Campos-Delgado, F. Lopez-Urias, Y. I. Vega-Cantu, F. J. Rodriguez-Macias, A. L. Elias, E. Munoz-Sandoval, A. G. Cano-Marquez, J. C. Charlier, H. Terrones, *Nano Today* **2010**, *5*, 351.
[18] N. L. Yang, J. Zhai, D. Wang, Y. S. Chen, L. Jiang, *ACS Nano* **2010**, *4*, 887.
[19] S. R. Sun, L. Gao, Y. Q. Liu, *Appl. Phys. Lett.* **2010**, 96.
[20] Y. B. Tang, C. S. Lee, J. Xu, Z. T. Liu, Z. H. Chen, Z. B. He, Y. L. Cao, G. D. Yuan, H. S. Song, L. M. Chen, L. B. Luo, H. M. Cheng, W. J. Zhang, I. Bello, S. T. Lee, *ACS Nano* **2010**, *4*, 3482.
[21] T. Sawatsuk, A. Chindaduang, C. Sae-Kung, S. Pratontep, G. Tumcharern, *Diamond Relat. Mater.* **2009**, *18*, 524.
[22] A. J. Bard, L. R. Faulkner, *Electrochemical Methods-Fundamentals and Applications*, 2nd ed., John Wiley & Sons, Inc. , New York **2000**.
[23] J. van de Lagemaat, N. G. Park, A. J. Frank, *J, Phys, Chem, B* **2000**, *104*, 2044.
[24] M. Adachi, M. Sakamoto, J. T. Jiu, Y. Ogata, S. Isoda, *J. Phys. Chem. B* **2006**, *110*, 13872.
[25] C. M. Li, W. Chen, X. Yang, C. Q. Sun, C. Gao, Z. X. Zheng, J. Sawyer, *Front. Biosci.* **2005**, *10*, 2518.
[26] R. Kern, R. Sastrawan, J. Ferber, R. Stangl, J. Luther, *Electrochim. Acta* **2002**, *47*, 4213.
[27] M. D. McGehee, *MRS Bull.* **2009**, *34*, 95.
[28] C. M. Li, C. Q. Sun, S. Song, V. E. Choong, G. Maracas, X. J. Zhang, *Front. Biosci.* **2005**, *10*, 180.
[29] S. R. Sun, L. Gao, Y. Q. Liu, *Appl. Phys. Lett.* **2010**, 96.
[30] P. Brown, K. Takechi, P. V. Kamat, *J. Phys. Chem. C* **2008**, *112*, 4776.
[31] C. X. Guo, H. B. Yang, Z. M. Sheng, Z. S. Lu, Q. L. Song, C. M. Li, *Angew. Chem. Int. Ed.* **2010**, *49*, 3014.
[32] W. S. Hummers, R. E. Offeman, *J. Am. Chem. Soc.* **1958**, *80*, 1339.